Metal artifact reduction techniques in musculoskeletal CT-imaging

Wellenberg, R. H. H.; Hakvoort, E. T.; Slump, C. H.; Boomsma, M. F.; Maas, M.; Streekstra, G. J.

Published in:
European journal of radiology

DOI:
10.1016/j.ejrad.2018.08.010

Published: 01/01/2018

Document Version
Publisher's PDF, also known as Version of record

Citation for pulished version (APA):
Wellenberg, R. H. H., Hakvoort, E. T., Slump, C. H., Boomsma, M. F., Maas, M., & Streekstra, G. J. (2018). Metal artifact reduction techniques in musculoskeletal CT-imaging. *European journal of radiology*, *107*, 60-69. https://doi.org/10.1016/j.ejrad.2018.08.010

European Journal of Radiology 107 (2018) 60–69

Contents lists available at ScienceDirect

European Journal of Radiology

journal homepage: www.elsevier.com/locate/ejrad

Review

Metal artifact reduction techniques in musculoskeletal CT-imaging

R.H.H. Wellenberg[a,b,*], E.T. Hakvoort[d], C.H. Slump[c], M.F. Boomsma[b], M. Maas[a], G.J. Streekstra[d]

[a] Department of Radiology and Nuclear Medicine, Amsterdam University Medical Center, location AMC, University of Amsterdam, Amsterdam Movement Sciences, Amsterdam, The Netherlands
[b] Department of Radiology, Isala, Zwolle, The Netherlands
[c] MIRA Institute for Biomedical Technology and Technical Medicine, University of Twente, Enschede, The Netherlands
[d] Department of Biomedical Engineering and Physics, Amsterdam University Medical Center, location AMC, Amsterdam, The Netherlands

ARTICLE INFO

Keywords:
Musculoskeletal CT
Metal artifacts
Metal artifact reduction software
Dual-energy CT
Virtual monochromatic imaging

ABSTRACT

It is known that metal artifacts can be reduced by modifying standard acquisition and reconstruction, by modifying projection data and/or image data and by using virtual monochromatic imaging extracted from dual-energy CT. In this review we focus on the origin of metal artifacts, technical background of commercially available metal artifact reduction (MAR) algorithms and the value of dual-energy CT and MAR software for different metal hardware in current clinical practice. Virtual monochromatic imaging reduces beam-hardening artifacts, where metal artifact reduction software effectively reduces artifacts caused by extensive photon-starvation. Both techniques have their advantages and disadvantages, and the combination of both techniques is often but not always the best solution regarding metal artifact reduction. Advances in prosthetic imaging are reinforced by advances in prosthetic design. Providing implant specific information prior to scanning is important in order to adjust the metal artifact reduction approach, minimize artifacts and optimize image quality and diagnostic value of CT.

1. Introduction

Major improvements in both image acquisition and reconstruction have been achieved in the past decades, which has lead to an increase in image quality in computed tomography (CT) [1]. Despite these technological advances, there are still artifacts that are not completely overcome. Artifacts, which are caused by metal implants, are present in different degrees of severity due to the variety of metals, shapes, and sizes used [2]. These artifacts impede the value and diagnostic accuracy of CT regarding the visualization of bone, bone-metal interfaces and soft tissue structures.

Contributors to metal artifacts are beam hardening, scatter, noise, photon starvation and edge effects [3] (Fig. 1). These contributions result in a reconstruction of near metal tissue using corrupted data, ultimately resulting in a wrong representation of the tissue. Analysis of tissue near metal therefore becomes unreliable and often impossible depending on the amount and composition of the metal in situ.

Beam hardening results in dark streaks between high attenuating objects [4]. The origin of this artifact lies in the fact that the x-ray beam is polychromatic i.e. does not consist of a single energy. When passing through matter, the photon flux will exponentially decrease. Due to the high density and high atomic number of most metals the absorption of low energies is substantial. This results in a hardened beam due to a detection of relatively few low-energy photons and many high-energy photons. The detector therefore detects too much energy which results in dark streaks after reconstruction if there are no or too little 'correct' projections available [5]. Scatter changes the direction of the incident photons. Reconstruction algorithms however, assume a straight line from tube to detector. In this way, the scattered photons end up in the wrong detector. The scattered photons add to the measured intensity and lead to an underestimation of the absorption and thus to dark streaks in the image, where white streaks are caused by an overestimation of the absorption. Photon starvation can be seen in high-density metals and in metals with a high atomic number. It leads to low photon counts and thus to increased noise and missing projection data. The background signal of the detector also adds to the noise level when no photons are detected at all [6]. This leads to dark streaks in the final reconstructed image where the metal is completely white. Edge effects can be observed at sharp edges between high and low attenuating tissues, for example an amalgam crown in the oral cavity. At those points the difference between the attenuation in infinitely small lines used in filtered back-projection (FBP) and the true x-ray beam is maximal. Edge

* Corresponding author at: Amsterdam University Medical Center, location AMC, Meibergdreef 9, 1105 AZ, Amsterdam, The Netherlands.
E-mail addresses: r.h.wellenberg@amc.uva.nl (R.H.H. Wellenberg), e.t.hakvoort@gmail.com (E.T. Hakvoort), c.h.slump@utwente.nl (C.H. Slump), m.f.boomsma@isala.nl (M.F. Boomsma), m.maas@amc.uva.nl (M. Maas), g.j.streekstra@amc.uva.nl (G.J. Streekstra).

https://doi.org/10.1016/j.ejrad.2018.08.010
Received 12 March 2018; Received in revised form 2 July 2018; Accepted 11 August 2018

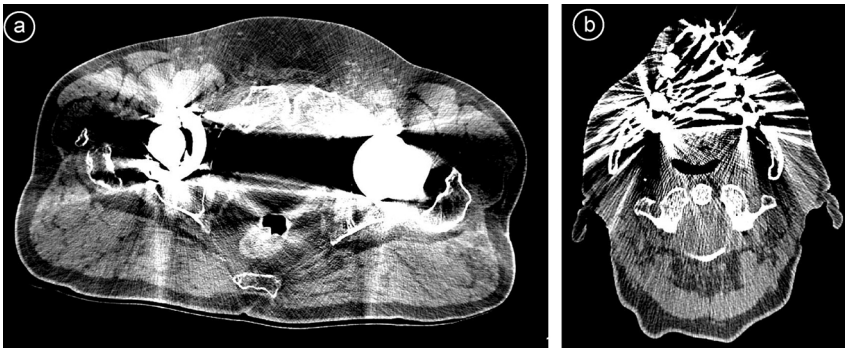

Fig. 1. a and b Beam hardening, photon starvation and scatter produce dark lines between hip replacements (1a, left). A combination of these artifacts originating from dental implants made of high molecular weight metals. (1b, right) (with courtesy of Isala, Zwolle, The Netherlands).

effects always leads to bright or dark lucent streaks [7] and therefore decrease the associated grey value along long edges. Noise, or the fluctuations in CT numbers of a uniform material, is generally not considered as an artifact although it has an effect on the final image. These fluctuations appear as graininess on CT images and are caused since the number of photons to form an image is limited [8].

In general, three steps can be distinguished in the CT reconstruction process: projection data acquisition, image reconstruction and post-processing. In all these steps, manipulations can be performed to improve the image quality and reduce metal artifacts. Metal artifact reduction (MAR) techniques focus on tackling these problems, either by minimizing the physical origin of the artifact or correcting for the artifacts in the image data or projection data. With current metal artifact reduction approaches, a totally new era of prosthetic imaging has started, since we are able to see the interface between the metallic surface and the osseous tissue. In this review we focus on the origin of metal artifacts, technical background of commercially available metal artifact reduction algorithms and the value of dual-energy CT and MAR software for different metal hardware in current clinical practice.

2. Metal artifact reduction strategies

Metal artifact reduction strategies are based on the reduction of all its primary causes i.e. beam hardening, scatter, photon starvation, noise, edge effects [7] and the combined effect. The chosen strategies can be categorized in three main approaches: 1) Modifying standard acquisition and reconstruction, 2) Modifying projection data and/or image data, 3) Applications of dual-energy CT (DECT). In our description and evaluation of the methods presented in literature we will follow this categorization.

2.1. Modifying standard acquisition and reconstruction

Increasing the kVp and mAs are traditional remedies to reduce the amount of metal artifacts. When increasing the average photon energy by increasing kVp, more photons will reach the detector since low-energy photons are more easily attenuated by metal objects than high-energy photons with a higher penetration. Furthermore, increasing the number of photons by increasing the mAs value will increase the number of photons that reach the detector thereby reducing noise and photon-starvation. Reducing the total collimation i.e. the detector width will reduce scatter. After image acquisition, the use of an extended Hounsfield Unit (HU) scale and use of a soft reconstruction kernel instead of a bone kernel reduces the visual conspicuity of metal artifacts [9].

By switching to more advanced iterative (IR) and model-based iterative reconstruction (MBIR) algorithms instead of standard FBP, more physical data and photon statistics is included in the reconstruction, which in theory minimizes scatter and edge effects by using correction algorithms [1,9]. In this way metal artifacts are reduced and overall image quality improves. Boudabbous et al. [10] investigated the value of MBIR compared to FBP regarding metal artifacts in 62 patients [10]. MBIR reduced metal artifacts and hence allowed an equal or better visibility of the bone-metal interfaces, as well as a better assessment of soft tissue around the metal implants. The size of the artifacts reduced and subjective image quality improved. Table 1 summarizes several ways to reduce metal artifacts by adjusting acquisition, reconstruction and visualization parameters [1,9,11–14]. It also summarizes advantages and disadvantages of the different measures taken.

Table 1
Adjusting acquisition, reconstruction and visualization parameters can reduce metal artifacts. Each of these adjustments has advantages and disadvantages.

	Advantage	Disadvantage
Acquisition		
• Increase tube current (mAs)	• Reduced photon-starvation	• Increased radiation exposure
• Increase tube voltage (kVp)	• Increased photon penetration	• Increased radiation exposure
• Reduce total collimation i.e. the detector width	• Reduced scatter and partial volume averaging	• Increased scan time
• Lower pitch	• Reduced image noise	• Increased radiation exposure when mAs is not adapted
Reconstruction		
• Use of (model-based) iterative reconstruction techniques	• Reduced amplification of artifacts	• Computationally intensive, possible reduced spatial resolution
• Change from bone to soft reconstruction kernel	• Reduced visual conspicuity of metal artifacts	• Reduced spatial resolution
• Increase slice thickness	• Reduced image noise	• Partial volume artifacts
Visualization		
• Use of an extended Hounsfield unit scale	• Reduced visual conspicuity of metal artifacts.	• Limited availability and compatibility and decreased contrast resolution

2.2. Modifying projection data and/or image data

2.2.1. General background of MAR algorithms

Several MAR algorithms have been developed the past decades. The basis of MAR techniques was presented by Kalender in 1987 who proposed an in-painting method which identifies the corrupted projection data caused by the presence of metal and subsequently replaces this corrupted projection data with averaged or interpolated data of neighboring detector elements [15]. To this end an uncorrected image is constructed from CT projection data or sinogram [16]. A metal image is subsequently created by means of thresholding. In this process all pixels with a higher value are considered to belong to the metal CT image. The metal image is forward projected into a metal sinogram, which is combined with the original sinogram. The new sinogram is back-projected to create a corrected image, which can be used as input for further corrections. Although this process reduces metal artifacts, it can also create new artifacts due to the limitations of thresholding yielding an imperfect new sinogram [17].

The use of an artifact free prior image can reduce the introduction of new artifacts [18]. A prior image is created by thresholding of the uncorrected image, with thresholds that correspond to air, soft tissue and bone tissue, in order to create a non-metal and metal image. The original sinogram pixel values are divided by the sinogram of the prior image in order to normalize it, which leads to homogeneous pixel values outside the metal trace. This results in an improved replacement of the metal by in-painting or by linear interpolation. Meyer et al. [19] showed that after de-normalization, a Normalized Metal Artifact Reduction (NMAR) image can be created by filtered back-projection and insertion of the metal image [19].

An improvement to this algorithm uses frequency splitting (FS) of the uncorrected and NMAR image [20]. This FSMAR algorithm combines a high frequency map of the uncorrected image domain and a low frequency map of the NMAR image domain. This FSMAR algorithm combines the near metal contrast of the uncorrected and NMAR image with the structural information of the NMAR image. In this way, all data from the more unreliable uncorrected image is combined with the more reliable NMAR image, which results in sharper edges.

A number of groups have developed refinements of MAR methods that are partly incorporated in commercially available algorithms of the main vendors including adaptive mixing [21,22], tissue modeling and adaptive filtering [23] and iterative frequency splitting [24]

2.2.2. Commercial MAR algorithms

Major vendors use iterative MAR algorithms (see Table 2). MAR software of Siemens (MAR in Image Space: MARIS and Iterative MAR: IMAR), Philips (Orthopedic MAR: O-MAR), GE (Smart MAR: MAR or MARS) and Toshiba (Single-Energy MAR: SEMAR) are all based on in-painting, in-painting with prior image, frequency splitting or a combination of these techniques [25–28]. However, detailed technical background information of vendor specific MAR approaches remains undisclosed.

Table 2
Dual-energy CT approaches, MAR algorithms and (model-based) iterative reconstruction techniques of different vendors [16].

	Dual-energy CT approach	MAR algorithm	(Model-based) Iterative reconstruction techniques
Siemens	Dual-source and TwinBeam	MARIS, IMAR	IRIS (1-5) Safire (1-5) Admire (1-5)[a]
Philips	Dual-layer detector	O-MAR	iDose[4] (1-7) IMR (1-3)[a]
GE	kV-switching	SMAR, MARS	ASIR (0-100%), ASIR-V (0-100%) Veo[a]
Toshiba	Dual-spin	SEMAR	AIDR (Mild, standard, strong) AIDR 3D (Mild, standard, strong) FIRST (Mild, standard, strong)[a]

[a] MBIR: Model-based iterative reconstruction.

Several groups published results using commercially available MAR algorithms from the four main vendors. Li et al. [29] investigated the orthopedic metal artifact reduction algorithm O-MAR on a 16-slice CT scanner regarding radiation therapy planning in a phantom and 10 patients with hip implants [29]. CT number accuracy and noise improved, especially in bilateral hip prosthesis and overall image quality and conspicuity of critical organs was significantly improved in O-MAR images compared to conventional images. Hilgers et al. [30] also found that CT number accuracy was better in O-MAR reconstructions in radiation therapy planning [30]. In patients with dental implants or fillings O-MAR images decreased noise and improved CT number accuracy compared to non-O-MAR images [31]. Furthermore, better qualitative scores were obtained in the streak artifacts regarding image sharpness, texture naturalness and degree of depiction. Boomsma et al. [32] and Wellenberg et al. [33,34] quantified the value of O-MAR in total hip arthroplasty imaging using a total hip arthroplasty phantom [32–34]. Overall image quality was improved when using model-based iterative reconstruction (IMR) technique compared to iterative and standard reconstruction. Combining IMR and O-MAR using 140-kVp resulted in the best overall image quality and most effective artifact reduction with improved CT number accuracy, lower noise values and higher signal-to-noise-ratios and contrast-to-noise-ratios [33].

When reducing CT radiation dose involving metal hardware, artifacts and noise are amplified since the number of photons that correctly end up the right detector is reduced. In a total hip arthroplasty phantom study, quantitative image quality parameters were maintained while reducing CT radiation dose up to 80% while using IMR with O-MAR compared to FBP with MAR. O-MAR was most effective in improving image quality in low-dose acquisitions, where metal artifacts were most pronounced [34]. In a similar phantom study, the use of MBIR with MAR software did not compromise the accuracy of lesion detectability near hardware while reducing CT radiation dose with 50% compared to FBP only. Furthermore, MBIR with MAR software was more sensitive in detecting smaller lesions and lesions near large amounts of artifacts [35]. Fig. 2 shows a clinical example of a patient with two large head metal-on-metal total hip arthroplasties with reduced metal artifacts in case of the O-MAR image. In patients with shoulder arthroplasties, Shim et al. [77] showed that O-MAR tends to degrade the depiction of bone trabeculae and bone cortex and generate new artifacts, including a pseudocemented appearance and scapular pseudonotching. They suggest using O-MAR complementary to non O-MAR images and not as a replacement.

Teixeira et al. [36] investigated iterative reconstruction in 24 unilateral en 24 bilateral hip patients, however with and without the use of SEMAR. When SEMAR was associated with IR, the gluteus minimus and medius tendons, obturator internus muscle, prostate or uterus and bladder could be visualized with medium or high confidence. The MAR technique appeared particularly useful when large amounts of metal were present [36]. These results were supported by Yasaka et al. [37] focusing on 28 patients with metal hip prostheses and Sonoda et al. [38] focusing on SEMAR and its value in 58 patients with hip prosthesis and embolization coils [37,38]. Regarding dental prosthesis SEMAR did not contribute significantly [38].

The added value of IMAR was investigated by Subhas et al. [26] in 8 patients with total shoulder athroplasties [26]. In a subsequent study, FBP and FBP with IMAR images of 40 shoulder patients and 21 hip patients were compared preoperatively and postoperatively [39]. IMAR resulted in more accurate CT values, a qualitative better image quality and less streak artifacts compared to non-IMAR results. Also, in a phantom, the readers detected more lesions with higher confidence. However, low contrast lesions located close to the head of the prosthesis were not detected. In spinal implants, Kotsenas et al. [40] and Aissa

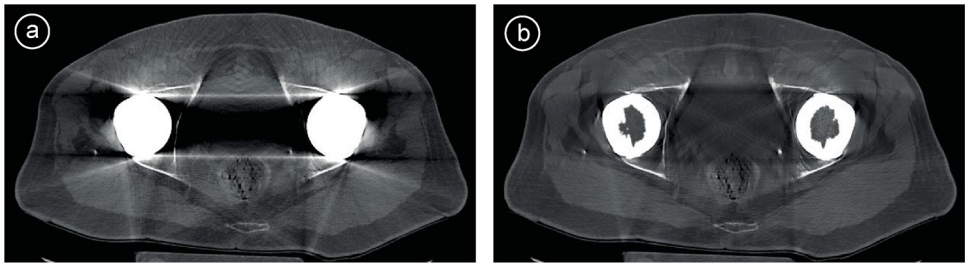

Fig. 2. Large head bilateral Metal-on-Metal total hip arthroplasties a) without and b) with the use of O-MAR. Images were acquired at 140 kVp and reconstructed using iterative reconstruction iDose^4 level 4 (with courtesy of Isala, Zwolle, The Netherlands).

Fig. 3. Dual-source Sn150/100 kVp virtual monochromatic images extracted at a) 40 keV, b) 70 keV, c) 130 keV and d) 190 keV in a patient with a suspected non-union of the femur fixated with a titanium intramedullary nail (with courtesy of the Academic Medical Center, Amsterdam, The Netherlands).

et al. [41] found that IMAR improved the visualization of surrounding critical soft tissues [40,41]. Severe artifacts caused by dental amalgam hardware and other hardware in the head and neck region were reduced using IMAR [42,43]. However, secondary artifacts emerged.

Wagenaar et al. [44] investigated several commercial MAR techniques in an anthropomorphic head and neck phantom. In addition to each scanners' own MAR technique, the reconstructed scans with metal artifacts were reconstructed using a metal deletion technique (MDT). This technique was developed by Boas et al. [6] and is based on reconstructed images instead of sinogram data [6]. HU errors were best reduced by O-MAR, followed by SMAR and Siemens' metal artifact reduction in image space (MARIS). MDT was found to be more effective in reducing HU errors than the commercial MAR techniques [44]. Another comparative phantom study by Bolstad et al. [45] focused on single energy CT with MAR software of the four main vendors. All approaches reduced metal artifacts and despite the fact that different reconstruction kernels were used the effect was most obvious for SEMAR compared to IMAR, O-MAR and SMAR and in stainless steel and cobalt chromium implants compared to titanium implants. Regarding titanium implants, new and more severe artifacts were introduced by the MAR algorithms [45].

2.3. Applications of dual-energy CT

DECT is a method for creating CT images which dates back to 1977 already [46]. In contrast to conventional CT, DECT reconstructs images acquired with two photon spectra at different kVp's. In the early days two scans were made sequentially which induced several artifacts such as partial volume and breathing artifacts due to movement. Nowadays, the spectra are created by either fast kV-switching of tube voltage (GE), having multiple tubes (Siemens), using a dual-layer detector (Philips) or using a beam split filter (Siemens) [16,47,48]. After the projection data has been recorded there are two ways of reconstructing an image. The first method creates virtual monochromatic images by reconstruction from two simultaneously acquired and processed projection data sets [47,49]. The other method creates virtual monochromatic images in the image domain [50,51] from separately reconstructed images at the two kVp levels. Virtual monochromatic images are useful since these images represent reconstructions at arbitrary average energies, which allows for contrast optimization and artifact reduction. By extrapolating to higher virtual monochromatic energies, the influence of low-energy photons becomes smaller and thus less beam hardening artifacts will arise [52,53], which is illustrated in Fig. 3. Currently there is no comparative data available which of the different DECT approaches is most effective in reducing metal artifacts.

Optimal monochromatic energies (keV) vary for different kind of metal hardware. Table 3 provides an overview of phantom and patient studies focusing on the reduction of metal artifacts using different DECT approaches and metal hardware with varying optimal keV's.

Various groups have shown that DECT is capable of reducing metal artifacts focusing on metal hardware in general [27,54–58], spine implants [48,59–62], osteosynthetic fixation implants [12,63,64], hip prosthesis [11,55,65–72] and dental implants [65,66,73,74]. Table 3 shows that there is no generalized optimal keV regarding metal hardware. These discrepancies in keV's might be explained by the differences in metal alloy, shape and size or geometry of the implant, body

Table 3
a and b Overview of DECT studies focusing on MAR (a) without the use of MAR software and (b) with the use additional MAR software.

a) DECT with no MAR software	Dual-energy approach	Optimal keV and investigated range	Patients	Phantom
Bamberg et al. [56]	Dual-source 100-140 kVp	119.5 ± 13.5 keV (95-150 keV) Range: 64-190 keV	Patients (n = 31) with various metal hardware	–
Zhou et al. [64]	Dual-source 80-140 kVp	130 keV Range: 40-190 keV	Patients (n = 47) with various fixation implants in the extremities and vertebrae	–
Meinel et al. [55]	Dual-source 80-140 kVp and 100-140 kVp	113 keV (100-130 keV) Range: 64-190 keV	Patients (n = 22) with various metal hardware	Phantom with titanium and steel hip prosthesis
Guggenberger et al. [61]	Dual-source 100-140 kVp	123-141 keV Range: 64-190 keV	–	Phantom with titanium spinal fusion implants
Lewis et al. [11]	Dual-source 100-140 kVp	150 keV Range: 40-190 keV	–	Phantom with different total hip replacements and a Catphan 500 phantom
Mangold et al. [63]	Sequential scanning 80 and 140 kVp	Only 130 keV was used	Patients (n = 50) with implants after osteosynthetic fracture treatment	–
Komlosi et al. [48]	kV-switching 80-140 kVp	> 90 keV titanium, > 110 keV cobalt chromium Range: 70-130 keV	–	Phantom with titanium and cobalt chromium spinal fixation rods
Filograna et al. [54]	Dual-source 100-140 kVp	137.1 ± 4.9 keV (130-148 keV) Range: 64-190 keV	Post mortem (n = 20) with various metal hardware	–
Higashigaito et al. [72]	Dual-source 100-150 kVp versus IMAR	84-143 keV Range: 40-190 keV	–	Pelvis phantom with unilateral and bilateral stainless steel and titanium inserts
Dong et al. [59]	kV-switching 80-140 kVp	120 keV Range: 60-140 keV	Patients (n = 45) with titanium spine screws	–
Wellenberg et al. [68]	Dual-layer detector 120 kVp and 140 kVp	74-150 keV Range: 74-200 keV	–	Phantom with TiAlV and CoCrMo total hip prosthesis
Neuhaus et al. [57]	Dual-layer detector 120 kVp	149.2 ± 39.4 keV (140 keV) Range: 64-200 keV	Patients (n = 35) with various metal hardware	–
Hokamp et al. [62]	Dual-layer detector 120 kVp versus O-MAR	Subjective 140 keV, objective 200 keV Range: 40-200 keV	Patients (n = 28) with orthopedic implants in the spine	–

b) DECT with MAR software	Dual-energy approach	Optimal keV and investigated range	Patients	Phantom
Lee et al. [27]	kV-switching + MAR 80-140 kVp	80 keV titanium, 110 keV stainless steel Range: 40-140 keV	Patients (n = 26) with various metal hardware	Phantom with a titanium and stainless steel fixation plate
Wang et al. [60]	kV-switching + MAR 80-140 kVp	110-140 keV Range: 65-140 keV	Patients (n = 18) with titanium pedicle spine screws	–
Han et al. [70]	kV-switching + MAR 80-140 kVp	No optimal keV provided Range: 40-140 keV	Patients (n = 53) with different metal hip prosthesis and screws at the femur neck	Pelvis phantoms with small bladder lesions and metal hip prostheses
Wang et al. [67]	kV-switching + MAR 80-140 kVp	110-120 keV Range: 70-140 keV	Patients (n = 23) with CoCrMo total hip prosthesis	–
Dabirrahmani et al. [75]	kV-switching + MAR 80-140 kVp	140 keV Range: 60-140 keV	–	Phantoms with cobalt chromium, titanium and stainless steel implants
Huang et al. [66]	kV-switching + MAR 80-140 kVp	Only 140 keV was used	–	Hip, dental, and thoracic phantoms with titanium, aluminum, stainless steel, cerrobend insertions
De Crop et al. [73]	kV-switching + MAR 80-140 kVp	No optimal keV could be identified Range: 40-140 keV	Dental cadaver with CoCr, Ti and Zr insertions	Catphan phantom with a CoCr cylindrical insertion
Andersson et al. [69]	kV-switching + MAR 80-140 kVp Dual-source + MAR 100-140 kVp	Only 110 keV was used	–	Phantom with cobalt chromium hip prosthesis
Bongers et al. [65]	Dual-source + MAR 100-140 kVp	Only 130 keV was used	Patients (n = 46) with various hip and dental hardware	–
Reynoso et al. [58]	kV-switching + MAR 80-140 kVp	Only 140 keV was used	Patients (n = 80) with various metal hardware	–
Cha et al. [74]	kV-switching + MAR 80-140 kVp	70-110 keV Range: 40-140 keV	Patients (n = 20) with metallic dental prostheses	–
Yue et al. [71]	kV-switching + MAR 80-140 kVp	120-140 keV Range: 80-140 keV	Patients (n = 35) with stainless steel and titanium unilateral hip arthroplasties	–

region and used acquisition parameters.

Meinel et al. [55] showed that when using tin (Sn) filtered dual-source CT, Sn140/80kVp was inferior to Sn140/100kVp when scanning the neck of steel hip prostheses. In DECT a greater difference in tube voltages enhances the spectral separation, which can also be valuable in other DECT applications. However regarding artifacts, the use of a lower kVp for one of the two tubes increases the presence of metal artifacts in the resultant images [55]. This is presumably caused by the

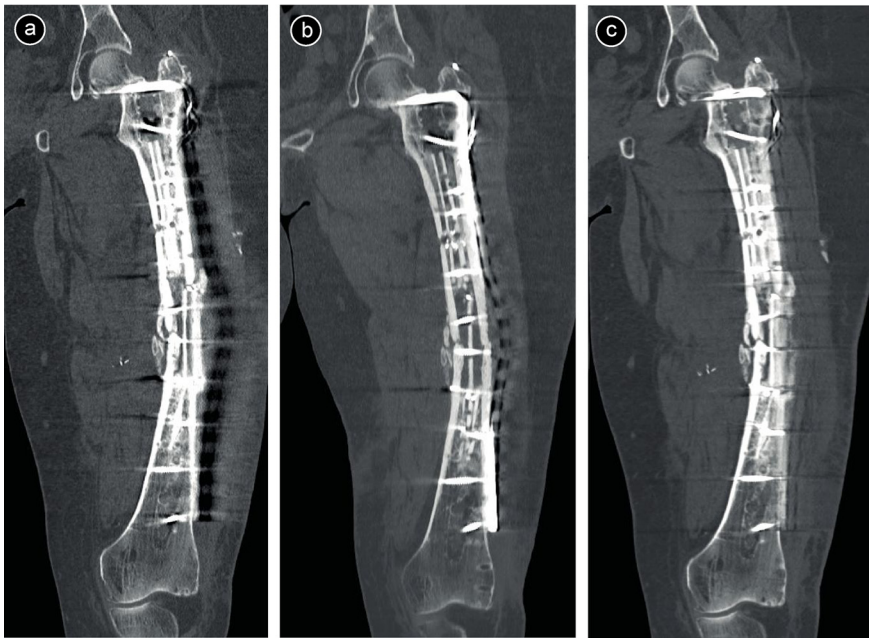

Fig. 4. Images of a patient with a suspected non-union of the femur treated with a stainless-steel fixation implant are shown. Fig. 4a/b illustrate a conventional 120-kVp image reconstructed a) without iMAR and b) with iMAR. Fig. 4c illustrates a 150 keV monochromatic image acquired with Sn150/100 kVp dual-source CT, 2 months prior to the conventional CT image shown in Fig. 4a and b (with courtesy of the Academic Medical Center, Amsterdam, The Netherlands).

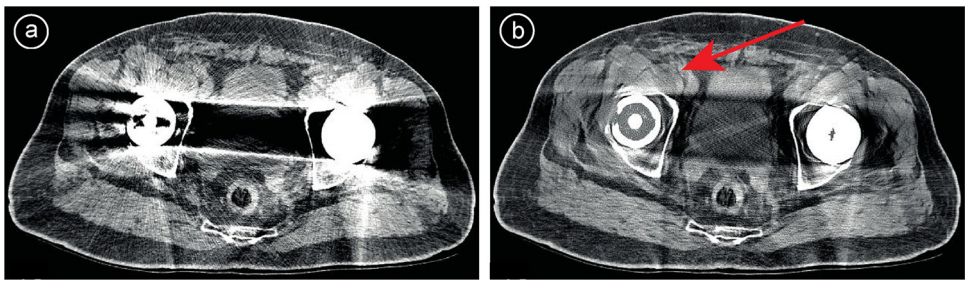

Fig. 5. In this patient with bilateral total hip arthroplasties, pseudo-tumor formation due to distension of the bursa iliopectinea on the right side in relation to the THA could easily be missed on the conventional CT images shown in Fig. 5a. In Fig. 5b, the use of additional MAR software enhances the visibility of this soft tissue pathology, indicated by the red arrow (with courtesy of Isala, Zwolle, The Netherlands).

fact that low-energy photons are more easily attenuated than high-energy photons. Lewis et al. [11] measured CT values and standard deviations in a hip phantom with gelatin and a Catphan phantom. No loss of high contrast line pair resolution was observed with no significant loss of spatial resolution while reducing streak artifacts up to 74% at 150 keV [11].

Several DECT studies confirmed that light metal alloys such as titanium generally cause far less artifacts than heavier metals such as stainless steel and cobalt chromium alloys [27,48,55,66,68,72]. Furthermore an increasing diameter or length of the metal hardware results in increased artifact severity [61]. The use of additional MAR software maintains mandatory in severe artifacts in order to reduce extensive photon starvation and scatter. Neuhaus et al. [57] found that in general 140 keV was optimal, however that in 20% of the cases higher keV's were chosen. Regarding hip prostheses, 200 keV was selected as the optimal image for all cases. In total hip prosthesis and especially in bilateral prosthesis there is no or little artifact reduction observed when using virtual monochromatic imaging only [65–68,72]. In these severe artifacts caused by bilateral hip prostheses and unilateral steel prostheses, IMAR outperformed monochromatic imaging [72]. Groβe Hokamp et al. [62] state that O-MAR and virtual monochromatic imaging both result in a significant reduction of metal artifacts with no clear superiority of one method over the other. Regarding O-MAR however, the introduction of new artifacts was observed in some cases [62]. As with conventional CT imaging, reducing CT radiation dose also increases metal artifact severity in THA imaging using dual-energy CT [68].

Fig. 4 illustrates that both MAR software and DECT reduce metal artifacts effectively in a patient with a suspected non-union of the femur treated with a stainless-steel fixation implant. Acquiring virtual monochromatic DECT images is not feasible on old generation CT scanners. On these systems, being able to use MAR software is essential, especially in patients with total hip arthroplasties in order to enhance the visibility of soft tissue and bone pathology (Fig. 5). Despite the fact that secondary artifacts could be introduced in smaller and lightweight metal hardware using MAR software on conventional CT systems, artifacts are reduced effectively and its use is more beneficial than not using MAR software at all.

2.4. The use of MAR and DECT

A logical step in further reducing of metal artifacts is the combination of dual-energy CT as an acquisition technique and MAR algorithms for post-processing. Several studies investigated the combined use of virtual monochromatic imaging and MAR software, which are summarized in Table 3b.

The value of Gemstone Spectral Imaging (GSI) combined with MAR software (MARS) is investigated in several patient and phantom studies [27,58,60,67,70,71,74,75]. In a phantom study Lee et al. [27] found that the combination of GSI and MARS is effective for the visualization of stainless steel prosthesis. Regarding titanium prosthesis the value of MARS additional to GSI may be limited [27]. In a study by Han et al. [70], radiologists judged the image quality of GSI with MARS to be much better than normal GSI in different types of metal hip prostheses in the pelvic cavity [70]. Image quality improved even though secondary artifacts were created where in some cases the image quality was even worse with MARS than without [70]. Wang et al. [67] confirmed these outcomes stating that in certain cases GSI without MARS

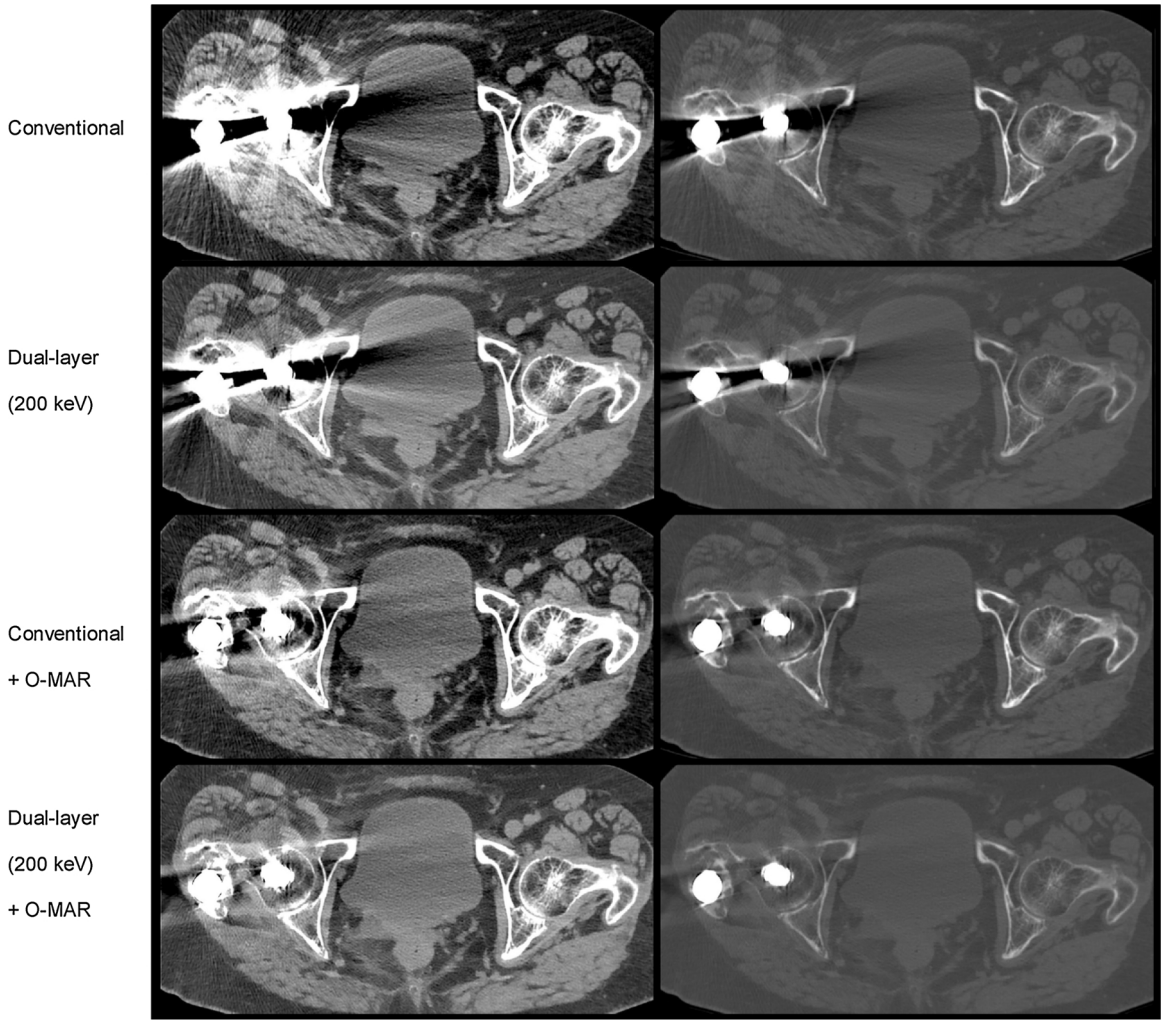

Fig. 6. 120 kVp conventional CT, dual-layer CT (200 keV), conventional + O-MAR and dual-layer CT (200 keV) + O-MAR in soft tissue window (width 350/ level 40, left) and bone window (width 1600/ level 400, right) (with courtesy of Cliniques Universitaires St-Luc, UCL Brussels).

resulted in more reliable images for clinical situations in patients with cobalt chromium hip prosthesis [67]. Artifacts were most effectively reduced at 140 keV, which was the highest energy investigated. Comparable results were found by Yue et al. [71], focusing on patients with unilateral hip arthroplasties and Dabirrahmani et al. [75] investigating phantoms with cobalt chromium, titanium and stainless steel implants [71,75]. Regarding titanium pedicle screws, Wang et al. [60] found that the width of the screws was measured with little errors above 100 keV. The shape of the screws was slightly distorted in MARS reconstructions which could not satisfy the clinicians [60]. Also results of this study showed that MARS did not always perform better. In 80 patients with metal implants in various regions, Reynoso et al. [58] found that periprosthetic monochromatic 140 keV images with MARS were better than monochromatic imaging alone regarding bone, fat and soft tissue. Results showed that energy levels should be adjusted to each tissue type and anatomic area in order to achieve an optimal performance in the evaluation of attenuation levels. Also in this study the image quality and interpretability was better, despite the presence of secondary artifacts [58]. Concerning patients with metallic dental prosthesis, Cha et al. [74] found that MARS with moderate keV reconstruction between 70–100 keV showed the best results [74]. Above 100 keV a plateau pattern of the artifacts was seen with decreased tissue contrast.

In 2015, Bongers et al. combined 130 keV DECT with IMAR on hip prosthesis and dental implants [65]. Clinicians agreed that the combination of IMAR and DECT reduced the metal artifacts the most. IMAR performed better than just DECT while both were better than single energy CT in both hip prosthesis and dental implants [65]. With respect to the oral cavity, De Crop et al. [73] investigated the effect of kVp, iterative reconstruction, DECT and MAR algorithms [73]. Dental fillings were simulated by inserting cylindrical implants of CoCr, Ti and Zr of 4 mm diameter and 10 mm length in a cadaver. Zirconium was found to cause the biggest artifact area, artifact index and standard deviation, followed by CoCr and Ti. Model-based iterative reconstruction leads to an increased image quality as well as a smaller artifact index. Increasing the keV reduced the artifact area while this effect was not so clear when the MAR algorithm was included. In most cases, including the MAR algorithm lead to a worse image quality. [73].

Comparisons of DECT and MAR approaches from different vendors were made by Huang et al. [66] and Andersson et al. [69]. The first group investigated the value of DECT and SECT combined with MAR in a phantom with bilateral cobalt chromium hip prosthesis in different vendors [69]. The use of DECT alone appeared to be insufficient and did in some cases increase the noise in the space between the prosthesis. MAR combined with conventional and dual-energy CT did reduce noise significantly. Secondary artifacts were introduced and these secondary artifacts were particularly obvious when the SEMAR algorithm was combined with IR [69]. Three metal artifact reduction methods including the O-MAR algorithm using SECT and monochromatic GSI and GSI with MARS were compared by Huang et al. [66]. The MAR approaches were tested on implant size, artifact reduction capability and

CT number accuracy using a hip prosthesis, dental and thoracic phantom with aluminum, stainless steel, titanium and cerrobend insertions. CT number accuracy became worse from titanium to unilateral stainless steel and bilateral stainless steel respectively for all MAR methods, which improved substantially in 140 keV images. GSI MARS performed almost 10% better than Philips O-MAR and GSI without MARS. All methods were able to reduce the metal artifacts created by hip prosthesis but were most successful for spinal fixation rods. However, none of the methods showed good results for metal artifact reduction in the dental cavity since the MAR algorithms created secondary artifacts, which lead to a greater error in Hounsfield units [66].

In general, the combination of MAR software and virtual monochromatic imaging can further reduce metal artifacts (Fig. 6), but it can also affect the appearance of metal implants [27,66,76], over or underestimate the size of the implant [75,76] or introduce secondary artifacts [58,66,69,70,76]. Advances in prosthetic imaging are reinforced by advances in prosthetic design itself. By improving the geometry, using smaller and lightweight implants or using metal substitutes, the presence of artifacts could be reduced in the first place.

3. Conclusions

In musculoskeletal CT imaging, adjusting acquisition, reconstruction and visualization parameters and the use of monochromatic DECT imaging with or without additional MAR software reduces metal artifacts produced by metal hardware. In addition, MBIR also reduces metal artifacts and improves overall image quality. Regarding its value in musculoskeletal CT imaging, further research is essential since images may appear too smooth and the possible reduction of spatial resolution may result in a loss of small details and affect the appearance of clinical findings such as fractures. DECT is able to reduce beam-hardening artifacts but not scatter, photon starvation and edge effects. It is difficult to define a general optimal keV. However, most studies find keV's in the range of 110–150 keV where 130 keV is sufficient for most small implants composed of lightweight alloys. Implementation of implant specific optimal keV's can be valuable to provide sufficient MAR while not degrading overall image contrast too much at high keV's. DECT artifact reduction is less effective for increasing molecular weight metals, larger implants and metals with sharp edges. Switching to higher keV's might provide some additional artifact reduction, however in these cases MAR software is advised. The combined use of DECT with MAR software is often but not always the best solution since MAR software tends to introduce new artifacts in case of lightweight metals. We strongly recommend evaluating conventional non-MAR reference images next to MAR images due to the possible introduction of these secondary artifacts. Furthermore, the irregular shape and high density of dental implants and coils seems to be problematic for most algorithms. In those cases both techniques fail to remove the artifacts.

Since metal artifacts differ due to differences in size, geometry and alloys of metal hardware, clinicians should be encouraged to provide implant specific information to the radiologist prior to scanning in order to adjust the metal artifact reduction approach, minimize artifacts and optimize image quality and diagnostic value of CT.

Disclosures of conflicts of interest

Each author certifies that he or she has no conflicts of interest to disclose.

References

[1] L. Gjesteby, B. De Man, Y. Jin, H. Paganetti, J. Verburg, D. Giantsoudi, et al., Metal Artifact Reduction in CT: Where Are We After Four Decades? IEEE 4 (2016) 5826–5849, https://doi.org/10.1109/ACCESS.2016.2608621.

[2] I. Gotman, Characteristics of Metals Used in Implants 11 (1997) 383–389.

[3] F.E. Boas, D. Fleischmann, CT artifacts: causes and reduction techniques, Imaging Med. 4 (2012) 229–240, https://doi.org/10.2217/iim.12.13.

[4] B. De Man, J. Nuyts, P. Dupont, G. Marchal, P. Suetens, Reduction of metal streak artifacts in x-ray computed tomography using a transmission maximum a posteriori algorithm, IEEE Trans. Nucl. Sci. 47 (2000) 977–981.

[5] R. Schulze, U. Heil, D. Groß, D.D. Bruellmann, E. Dranischnikow, U. Schwanecke, et al., Artefacts in CBCT: a review, Dentomaxillofacial Radiol. 40 (2011) 265–273, https://doi.org/10.1259/dmfr/30642039.

[6] F.E. Boas, D. Fleischmann, Evaluation of two iterative techniques for reducing metal artifacts in computed tomography, Radiology. 259 (2011) 894–902, https://doi.org/10.1148/radiol.11101782.

[7] P.M. Joseph, R.D. Spital, The exponential edge-gradient effect in X-ray computed tomography, Phys. Med. Biol. 26 (1981) 473–487, https://doi.org/10.1088/0031-9155/26/3/010.

[8] L.W. Goldman, Principles of CT and CT technology, J. Nucl. Med. Technol. 35 (2007), https://doi.org/10.2967/jnmt.107.042978 115-28-30.

[9] P.I. Mallinson, T.M. Coupal, P.D. McLaughlin, S. Nicolaou, P.L. Munk, H.A. Ouellette, Dual-energy CT for the musculoskeletal system, Radiology 281 (2016) 690–707, https://doi.org/10.1148/radiol.2016151109.

[10] S. Boudabbous, D. Arditi, E. Paulin, A. Syrogiannopoulou, C. Becker, X. Montet, Model-based iterative reconstruction (MBIR) for the reduction of metal artifacts on CT, Am. J. Roentgenol. 205 (2015) 380–385, https://doi.org/10.2214/AJR.14.13334.

[11] M. Lewis, K. Reid, A. Toms, Reducing the effects of metal artefact using high keV monoenergetic reconstruction of dual energy CT (DECT) in hip replacements, Skeletal Radiol. 42 (2013) 275–282, https://doi.org/10.1007/s00256-012-1458-6.

[12] T.M. Coupal, P.I. Mallinson, P. McLaughlin, S. Nicolaou, P.L. Munk, H. Ouellette, Peering through the glare: using dual-energy CT to overcome the problem of metal artefacts in bone radiology, Skeletal Radiol. 43 (2014) 567–575, https://doi.org/10.1007/s00256-013-1802-5.

[13] K.A. Buckwalter, J.A. Parr, R.H. Choplin, W.N. Capello, Multichannel CT imaging of orthopedic hardware and implants, Semin. Musculoskelet. Radiol. 10 (2006) 86–97, https://doi.org/10.1055/s-2006-934219.

[14] T. Do, R. Sutter, S. Skornitzke, M.-A. Weber, CT and MRI techniques for imaging around orthopedic hardware, RöFo - Fortschritte Auf Dem Gebiet Der Röntgenstrahlen Und der bildgeb, Verfahren 190 (Jan(1)) (2018) 31–41, https://doi.org/10.1055/s-0043-118127.

[15] W.A. Kalender, R. Hebel, J. Ebersberger, Reduction of CT artifacts caused by metallic implants, Radiology 164 (1987) 576–577, https://doi.org/10.1148/radiology.164.2.3602406.

[16] M.M. Lell, J.E. Wildberger, H. Alkadhi, J. Damilakis, M. Kachelriess, Evolution in Computed Tomography: The Battle for Speed and Dose, Invest. Radiol. 50 (2015) 629–644, https://doi.org/10.1097/RLI.0000000000000172.

[17] Y. Chen, Y. Li, H. Guo, Y. Hu, L. Luo, X. Yin, et al., CT metal artifact reduction method based on improved image segmentation and sinogram in-painting, Math. Probl. Eng. 2012 (2012) 1–19, https://doi.org/10.1155/2012/786281.

[18] R. Pua, S. Wi, M. Park, J.R. Lee, S. Cho, An image-based reduction of metal artifacts in computed tomography, J. Comput. Assist. Tomogr. 40 (2016) 131–141, https://doi.org/10.1097/RCT.0000000000000316.

[19] E. Meyer, F. Bergner, R. Raupach, T. Flohr, M. Kachelrieß, Normalized metal artifact reduction (NMAR) in computed tomography, Med. Phys. 37 (2009) 3251–3255, https://doi.org/10.1109/NSSMIC.2009.5401721.

[20] E. Meyer, R. Raupach, M. Lell, B. Schmidt, M. Kachelriess, M. Kachelrieß, Frequency split metal artifact reduction (FSMAR) in computed tomography, Med. Phys. 39 (2012) 1904, https://doi.org/10.1118/1.3691902.

[21] A.H. Mahnken, R. Raupach, J.E. Wildberger, B. Jung, N. Heussen, T.G. Flohr, et al., A new algorithm for metal artifact reduction in computed tomography, Invest. Radiol. 38 (2003) 769–775, https://doi.org/10.1097/01.rli.0000086495.96457.54.

[22] P.T. Liu, W.P. Pavlicek, M.B. Peter, M.J. Spangehl, C.C. Roberts, R.G. Paden, Metal artifact reduction image reconstruction algorithm for CT of implanted metal orthopedic devices: a work in progress, Skeletal Radiol. 38 (2009) 797–802, https://doi.org/10.1007/s00256-008-0630-5.

[23] M. Bal, L. Spies, Metal artifact reduction in CT using tissue-class modeling and adaptive prefiltering, Med. Phys. 33 (2006) 2852–2859, https://doi.org/10.1118/1.2218062.

[24] F. Morsbach, S. Bickelhaupt, G.A. Wanner, Reduction of metal artifacts from hip prostheses on CT images of the pelvis : value of iterative reconstructions, Radiology 268 (2013) 237–244, https://doi.org/10.1148/radiol.13122089.

[25] J. Bryniarski, White paper: Metal Artifact Reduction for Orthopedic Implants (O-MAR), (2012).

[26] N. Subhas, A.N. Primak, N.A. Obuchowski, A. Gupta, J.M. Polster, A. Krauss, et al., Iterative metal artifact reduction: Evaluation and optimization of technique, Skeletal Radiol. 43 (2014) 1729–1735, https://doi.org/10.1007/s00256-014-1987-2.

[27] Y.H. Lee, K.K. Park, H.-T. Song, S. Kim, J.-S. Suh, Metal artefact reduction in gemstone spectral imaging dual-energy CT with and without metal artefact reduction software, Eur. Radiol. 22 (2012) 1331–1340, https://doi.org/10.1007/s00330-011-2370-5.

[28] K. Sofue, T. Yoshikawa, N. Negi, Y. Ohno, N. Sugihara, H. Koyama, et al., Abdominal CT with single-energy metal artifact reduction (SEMAR): initial experiences, Sci. Exhib. ECR 2014 (2014) 1–16, https://doi.org/10.1594/ecr2014/C-0674.

[29] H. Li, C. Noel, H. Chen, H.H. Li, D. Low, K. Moore, et al., Clinical evaluation of a commercial orthopedic metal artifact reduction tool for CT simulations in radiation therapy, Med. Phys. 39 (2012) 7507–7517, https://doi.org/10.1118/1.4762814.

[30] G. Hilgers, T. Nuver, A. Minken, The CT number accuracy of a novel commercial metal artifact reduction algorithm for large orthopedic implants, J. Appl. Clin. Med. Phys. 15 (2014) 274–278, https://doi.org/10.1120/jacmp.v15i1.4597.

[31] M. Kidoh, T. Nakaura, S. Nakamura, S. Tokuyasu, H. Osakabe, K. Harada, et al., Reduction of dental metallic artefacts in CT: value of a newly developed algorithm for metal artefact reduction (O-MAR), Clin. Radiol. 69 (2014) e11–e16, https://doi.org/10.1016/j.crad.2013.08.008.
[32] M.F. Boomsma, N. Warringa, M.A. Edens, D. Mueller, H.B. Ettema, C.C.P.M. Verheyen, et al., Quantitative analysis of orthopedic metal artefact reduction in 64-slice computed tomography scans in large head metal-on-metal total hip replacement, a phantom study, Springerplus 5 (2016) 405, https://doi.org/10.1186/s40064-016-2006-y.
[33] R.H.H. Wellenberg, M.F. Boomsma, J.A.C. Osch van, J. Milles, A. Vlassenbroek, M.A. Edens, et al., Computed tomography imaging of a hip prosthesis using iterative model-based reconstruction and orthopaedic metal artefact reduction: a quantitative analysis, J. Comput. Assist. Tomogr. 40 (2016) 971–978, https://doi.org/10.1097/RCT.0000000000000449.
[34] R.H.H. Wellenberg, M.F. Boomsma, J.A.C. van Osch, J. Milles, A. Vlassenbroek, M.A. Edens, et al., Low-dose CT imaging of a total hip arthroplasty phantom using model-based iterative reconstruction and orthopedic metal artifact reduction, Skelet. Radiol. 46 (2017) 623–632, https://doi.org/10.1007/s00256-017-2580-2.
[35] N. Subhas, C.P. Pursyko, J.M. Polster, N.A. Obuchowski, A.N. Primak, F.F. Dong, et al., Dose reduction with dedicated CT metal artifact reduction algorithm: CT phantom study, Am. J. Roentgenol. 210 (2018) 593–600, https://doi.org/10.2214/AJR.17.18544.
[36] P. Gondim Teixeira, J. Meyer, C. Baumann, A. Raymond, F. Sirveaux, H. Coudane, et al., Total hip prosthesis CT with single-energy projection-based metallic artifact reduction: impact on the visualization of specific periprosthetic soft tissue structures, Skeletal Radiol. 43 (2014) 1237–1246, https://doi.org/10.1007/s00256-014-1923-5.
[37] K. Yasaka, E. Maeda, S. Hanaoka, M. Katsura, J. Sato, K. Ohtomo, Single-energy metal artifact reduction for helical computed tomography of the pelvis in patients with metal hip prostheses, J. Radiol. 34 (2016) 625–632, https://doi.org/10.1007/s11604-016-0566-y.
[38] A. Sonoda, N. Nitta, N. Ushio, Y. Nagatani, N. Okumura, H. Otani, et al., Evaluation of the quality of CT images acquired with the single energy metal artifact reduction (SEMAR) algorithm in patients with hip and dental prostheses and aneurysm embolization coils, J. Radiol. 33 (2015) 710–716, https://doi.org/10.1007/s11604-015-0478-2.
[39] N. Subhas, J.M. Polster, N.A. Obuchowski, A.N. Primak, F.F. Dong, B.R. Herts, et al., Imaging of arthroplasties: improved image quality and lesion detection with iterative metal artifact reduction, a new CT metal artifact reduction technique, Am. J. Roentgenol. 207 (2016) 378–385, https://doi.org/10.2214/AJR.15.15850.
[40] A.L. Kotsenas, G.J. Michalak, D.R. DeLone, F.E. Diehn, K. Grant, A.F. Halaweish, et al., CT metal artifact reduction in the spine: can an iterative reconstruction technique improve visualization? Am. J. Neuroradiol. 36 (2015) 2184–2190, https://doi.org/10.3174/ajnr.A4416.
[41] J. Aissa, C. Thomas, L.M. Sawicki, J. Caspers, P. Kröpil, G. Antoch, et al., Iterative metal artefact reduction in CT: can dedicated algorithms improve image quality after spinal instrumentation? Clin. Radiol. 72 (428) (2017), https://doi.org/10.1016/j.crad.2016.12.006 e7-428.e12.
[42] J. Weiß, C. Schabel, M. Bongers, R. Raupach, S. Clasen, M. Notohamiprodjo, et al., Impact of iterative metal artifact reduction on diagnostic image quality in patients with dental hardware, Acta Radiol. 58 (2016) 279–285, https://doi.org/10.1177/0284185116646144.
[43] F.E. Diehn, G.J. Michalak, D.R. DeLone, A.L. Kotsenas, E.P. Lindell, N.G. Campeau, et al., CT dental artifact: comparison of an iterative metal artifact reduction technique with weighted filtered back-projection, Acta Radiol. Open 6 (2017), https://doi.org/10.1177/2058460117743279 205846011774327.
[44] D. Wagenaar, E.R. Van Der Graaf, A. Van Der Schaaf, M.J.W. Greuter, Quantitative comparison of commercial and non-commercial metal artifact reduction techniques in computed tomography, PLoS One 10 (2015) 1–9, https://doi.org/10.1371/journal.pone.0127932.
[45] K. Bolstad, S. Flatabø, D. Aadnevik, I. Dalehaug, N. Vetti, Metal artifact reduction in CT, a phantom study: subjective and objective evaluation of four commercial metal artifact reduction algorithms when used on three different orthopedic metal implants, Acta Radiol. 0 (2018), https://doi.org/10.1177/0284185117751278 28418511775127.
[46] H.K. Genant, D. Boyd, Quantitative bone mineral analysis using dual energy computed tomography, Invest. Radiol. 12 (1977) 545–551, https://doi.org/10.1097/00004424-197711000-00015.
[47] T.R.C. Johnson, Dual-energy CT: general principles, AJR Am. J. Roentgenol. 199 (2012) 3–8, https://doi.org/10.2214/AJR.12.9116.
[48] P. Komlosi, D. Grady, J.S. Smith, C.I. Shaffrey, A.R. Goode, P.G. Judy, et al., Evaluation of monoenergetic imaging to reduce metallic instrumentation artifacts in computed tomography of the cervical spine, J. Neurosurg. Spine 22 (2015) 34–38, https://doi.org/10.3171/2014.10.SPINE14463.
[49] R.E. Alvarez, A. Macovski, Energy-selective reconstructions in X-ray computerized tomography, Phys. Med. Biol. 21 (1976) 733–744, https://doi.org/10.1088/0031-9155/21/5/002.
[50] L. Yu, J.A. Christner, S. Leng, J. Wang, J.G. Fletcher, C.H. McCollough, Virtual monochromatic imaging in dual-source dual-energy CT: radiation dose and image quality, Med. Phys. 38 (2011) 6371, https://doi.org/10.1118/1.3658568.
[51] L.A. Lehmann, R.E. Alvarez, A. Macovski, W.R. Brody, N.J. Pelc, S.J. Riederer, et al., Generalized image combinations in dual KVP digital radiography, Med. Phys. 8 (1981) 659–667, https://doi.org/10.1118/1.595025.
[52] K.L. Grant, T.G. Flohr, B. Krauss, M. Sedlmair, C. Thomas, B. Schmidt, Assessment of an advanced image-based technique to calculate virtual monoenergetic computed tomographic images from a dual-energy examination to improve contrast-to-Noise ratio in examinations using iodinated contrast media, Invest. Radiol. 49 (2014) 586–592, https://doi.org/10.1097/RLI.0000000000000060.
[53] S. Kuchenbecker, S. Faby, S. Sawall, M. Lell, M. Kachelrieß, Dual energy CT: how well can pseudo-monochromatic imaging reduce metal artifacts? Med. Phys. 42 (2015) 1023–1036, https://doi.org/10.1118/1.4905106.
[54] L. Filograna, N. Magarelli, A. Leone, R. Guggenberger, S. Winklhofer, M.J. Thali, et al., Value of monoenergetic dual-energy CT (DECT) for artefact reduction from metallic orthopedic implants in post-mortem studies, Skeletal Radiol. 44 (2015) 1287–1294, https://doi.org/10.1007/s00256-015-2155-z.
[55] F. Meinel, B. Bischoff, Q. Zhang, F. Bamberg, M. Reiser, T. Johnson, Metal artifact reduction by dual-energy computed tomography using energetic extrapolation: a systematically optimized protocol, Invest. Radiol. 47 (2012) 406–414, https://doi.org/10.1097/RLI.0b013e31824c86a3.
[56] F. Bamberg, A. Dierks, K. Nikolaou, M.F. Reiser, C.R. Becker, T.R. Johnson, Metal artifact reduction by dual energy computed tomography using monoenergetic extrapolation, Eur. Radiol. 21 (2011) 1424–1429, https://doi.org/10.1007/s00330-011-2062-1.
[57] V. Neuhaus, Metal artifact reduction by dual-layer computed tomography using virtual monoenergetic images, Eur. J. Radiol. 93 (2017) 143–148, https://doi.org/10.1016/j.ejrad.2017.05.013.
[58] E. Reynoso, C. Capunay, A. Rasumoff, J. Vallejos, J. Carpio, K. Lago, et al., Periprosthetic artifact reduction using virtual monochromatic imaging derived from gemstone dual-energy computed tomography and dedicated software, J. Comput. Assist. Tomogr. 40 (2016) 649–657, https://doi.org/10.1097/RCT.0000000000000399.
[59] Y. Dong, A.J. Shi, J.L. Wu, R.X. Wang, L.F. Sun, A.L. Liu, et al., Metal artifact reduction using virtual monochromatic images for patients with pedicle screws implants on CT, Eur. Spine J. 25 (2016) 1754–1763, https://doi.org/10.1007/s00586-015-4053-4.
[60] Y. Wang, B. Qian, B. Li, G. Qin, Z. Zhou, Y. Qiu, et al., Metal artifacts reduction using monochromatic images from spectral CT: evaluation of pedicle screws in patients with scoliosis, Eur. J. Radiol. 82 (2013) e360–e366, https://doi.org/10.1016/j.ejrad.2013.02.024.
[61] R. Guggenberger, S. Winklhofer, G. Osterhoff, Ga. Wanner, M. Fortunati, G. Andreisek, et al., Metallic artefact reduction with monoenergetic dual-energy CT: systematic ex vivo evaluation of posterior spinal fusion implants from various vendors and different spine levels, Eur. Radiol. 22 (2012) 2357–2364, https://doi.org/10.1007/s00330-012-2501-7.
[62] N. Große Hokamp, V. Neuhaus, N. Abdullayev, K. Laukamp, S. Lennartz, A. Mpotsaris, et al., Reduction of artifacts caused by orthopedic hardware in the spine in spectral detector CT examinations using virtual monoenergetic image reconstructions and metal-artifact-reduction algorithms, Skeletal Radiol. 47 (Feb(2)) (2018) 195–201, https://doi.org/10.1007/s00256-017-2776-5.
[63] S. Mangold, S. Gatidis, O. Luz, B. König, C. Schabel, M.N. Bongers, et al., Single-source dual-energy computed tomography, use of monoenergetic extrapolation for a reduction of metal artifacts, Invest. Radiol. 49 (2014) 788–793, https://doi.org/10.1097/RLI.0000000000000083.
[64] C. Zhou, Y.E. Zhao, S. Luo, H. Shi, L. li, L. Zheng, et al., Monoenergetic imaging of dual-energy CT reduces artifacts from implanted metal orthopedic devices in patients with factures, Acad. Radiol. 18 (2011) 1252–1257, https://doi.org/10.1016/j.acra.2011.05.009.
[65] M.N. Bongers, C. Schabel, C. Thomas, R. Raupach, M. Notohamiprodjo, K. Nikolaou, et al., Comparison and combination of dual-energy- and iterative- based metal artefact reduction on hip prosthesis and dental implants, PLoS One 10 (2015) 1–12, https://doi.org/10.1371/journal.pone.0143584.
[66] J. Huang, J. Kerns, J. Nute, X. Liu, P. Balter, F. Stingo, et al., An evaluation of three commercially available metal artifact reduction methods for CT imaging, Phys. Med. Biol. 60 (2015) 1047–1067, https://doi.org/10.1088/0031-9155/60/3/1047.
[67] F. Wang, H. Xue, X. Yang, W. Han, B. Qi, Y. Fan, et al., Reduction of metal artifacts from alloy hip prostheses in computer tomography, J. Comput. Assist. Tomogr. 38 (2014) 823–833, https://doi.org/10.1097/RCT.0000000000000125.
[68] R.H.H. Wellenberg, M.F. Boomsma, J.A.C. van Osch, J. Milles, A. Vlassenbroek, M.A. Edens, et al., Quantifying metal artefact reduction using virtual monochromatic dual-layer detector spectral CT imaging in unilateral and bilateraltotal hip prostheses, Eur. J. Radiol. 88 (2017) 61–70, https://doi.org/10.1016/j.ejrad.2017.01.002.
[69] K.M. Andersson, P. Nowik, J. Persliden, P. Thunberg, E. Norrman, Metal artefact reduction in CT imaging of hip prostheses-an evaluation of commercial techniques provided by four vendors, Br. J. Radiol. 88 (2015), https://doi.org/10.1259/bjr.20140473.
[70] S.C. Han, Y.E. Chung, Y.H. Lee, K.K. Park, M.J. Kim, K.W. Kim, Metal artifact reduction software used with abdominopelvic dual-energy CT of patients with metal hip prostheses: assessment of image quality and clinical feasibility, Am. J. Roentgenol. 203 (2014) 788–795, https://doi.org/10.2214/AJR.13.10980.
[71] D. Yue, C. Fan Rong, C. Ning, H. Liang, L. Ai Lian, W. Ru Xin, et al., Reduction of metal artifacts from unilateral hip arthroplasty on dual-energy CT with metal artifact reduction software, Acta radiol. 0 (2017), https://doi.org/10.1177/0284185117731475 28418511773147.
[72] K. Higashigaito, F. Angst, V.M. Runge, H. Alkadhi, O.F. Donati, Metal artifact reduction in pelvic computed tomography with hip prostheses: comparison of virtual monoenergetic extrapolations from dual-energy computed tomography and an iterative metal artifact reduction algorithmin a phantomstudy, Invest. Radiol. 50 (2015) 828–834, https://doi.org/10.1097/RLI.0000000000000191.
[73] A. De Crop, J. Casselman, T. Van Hoof, M. Dierens, E. Vereecke, N. Bossu, et al., Analysis of metal artifact reduction tools for dental hardware in CT scans of the oral cavity: kVp, iterative reconstruction, dual-energy CT, metal artifact reduction

software: does it make a difference? Neuroradiology. 57 (2015) 841–849, https://doi.org/10.1007/s00234-015-1537-1.
[74] J. Cha, H.J. Kim, S.T. Kim, Y.K. Kim, H.Y. Kim, G.M. Park, Dual-energy CT with virtual monochromatic images and metal artifact reduction software for reducing metallic dental artifacts, Acta Radiol. 58 (2017) 1312–1319, https://doi.org/10.1177/0284185117692174.
[75] D. Dabirrahmani, J. Magnussen, R.C. Appleyard, Dual-energy computed tomography - how accurate is gemstone spectrum imaging metal artefact reduction? Its application to orthopedic metal implants, J. Comput. Assist. Tomogr. 39 (Nov–Dec (6)) (2015) 925–935, https://doi.org/10.1097/RCT.0000000000000300.
[76] E. Pessis, J.M. Sverzut, R. Campagna, H. Guerini, A. Feydy, J.-L. Drapé, Reduction of metal artifact with dual-energy CT: virtual monospectral imaging with fast kilovoltage switching and metal artifact reduction software, Semin. Musculoskelet. Radiol. 19 (2015) 446–455, https://doi.org/10.1055/s-0035-1569256.
[77] E. Shim, Y. Kang, J.M. Ahn, E. Lee, J.W. Lee, J.H. Oh, et al., Metal artefact reduction for orthopedic implants (O-MAR): usefulness in CT evaluation of reverse total shoulder arthroplasty, Am. J. Roentgenol. 209 (2017) 860–866, https://doi.org/10.2214/AJR.16.17684.